applied sciences

MDPI

Article

Optimizing Power and Thermal Efficiency of an Irreversible Variable-Temperature Heat Reservoir Lenoir Cycle

Ruibo Wang [1,2,3], Lingen Chen [1,2,3,*], Yanlin Ge [1,2,3] and Huijun Feng [1,2,3]

1 Institute of Thermal Science and Power Engineering, Wuhan Institute of Technology, Wuhan 430205, China; ruibowq@126.com (R.W.); geyali9@hotmail.com (Y.G.); huijunfeng@139.com (H.F.)
2 Hubei Provincial Engineering Technology Research Center of Green Chemical Equipment, Wuhan 430205, China
3 School of Mechanical & Electrical Engineering, Wuhan Institute of Technology, Wuhan 430205, China
* Correspondence: lgchenna@yahoo.com or lingenchen@hotmail.com

Abstract: Applying finite-time thermodynamics theory, an irreversible steady flow Lenoir cycle model with variable-temperature heat reservoirs is established, the expressions of power (P) and efficiency (η) are derived. By numerical calculations, the characteristic relationships among P and η and the heat conductance distribution (u_L) of the heat exchangers, as well as the thermal capacity rate matching (C_{wf1}/C_H) between working fluid and heat source are studied. The results show that when the heat conductances of the hot- and cold-side heat exchangers (U_H, U_L) are constants, P-η is a certain "point", with the increase of heat reservoir inlet temperature ratio (τ), U_H, U_L, and the irreversible expansion efficiency (η_e), P and η increase. When u_L can be optimized, P and η versus u_L characteristics are parabolic-like ones, there are optimal values of heat conductance distributions ($u_{L_P(opt)}$, $u_{L_\eta(opt)}$) to make the cycle reach the maximum power and efficiency points ($P_{\max}$, $\eta_{\max}$). As C_{wf1}/C_H increases, $P_{\max}$-C_{wf1}/C_H shows a parabolic-like curve, that is, there is an optimal value of C_{wf1}/C_H ($(C_{wf1}/C_H)_{opt}$) to make the cycle reach double-maximum power point ($(P_{\max})_{\max}$); as C_L/C_H, U_T, and η_e increase, $(P_{\max})_{\max}$ and $(C_{wf1}/C_H)_{opt}$ increase; with the increase in τ, $(P_{\max})_{\max}$ increases, and $(C_{wf1}/C_H)_{opt}$ is unchanged.

Keywords: finite-time thermodynamics; irreversible steady-flow Lenoir cycle; cycle power; thermal efficiency; heat conductance distribution; thermal capacity rate matching

check for updates

Citation: Wang, R.; Chen, L.; Ge, Y.; Feng, H. Optimizing Power and Thermal Efficiency of an Irreversible Variable-Temperature Heat Reservoir Lenoir Cycle. *Appl. Sci.* **2021**, *11*, 7171. https://doi.org/10.3390/app11157171

Academic Editor: Xiaolin Wang

Received: 14 July 2021
Accepted: 30 July 2021
Published: 3 August 2021

1. Introduction

As a further extension of traditional irreversible process thermodynamics, finite-time thermodynamics (FTT) [1–11] has been applied to analyze and optimize performances of actual thermodynamic cycles, and great progress has been made. FTT has been applied in micro- and nano-cycles [12–15], thermoelectric devices [16,17], thermionic devices [18,19], gas turbine cycles [20–22], internal combustion cycles [23,24], cogeneration plants [25,26], thermoradiative cell [27], chemical devices [28,29], and economics [30,31].

According to the nature of the cycle, the researched heat engine (HEG) cycles include steady flow cycles [32–37] and reciprocating cycles [38–48]. For the steady flow HEG cycle, considering the temperature change of the heat reservoir (HR) can make the cycle closer to the actual working state of the HEG, therefore, some scholars have studied the steady flow cycles with variable temperature HR [49–53].

The Lenoir cycle (LC) model [54] was proposed by Lenoir in 1860. From the perspective of the cycle process, the LC lacks a compression process. It looks like a triangle in the cycle T-s diagram. It is a typical atmosphere pressure compression HEG cycle, the compression process required by the HEG during operation is realized by atmosphere pressure and it can be used in aerospace, ships, vehicles, and power plants in engineering practice. Georgiou [55] first used classical thermodynamics to study the steady flow Lenoir cycle (SFLC) and compared its performance with that of a steady flow Carnot cycle.

Compared to the classical thermodynamics, the finite time process of the finite rate heat exchange (HEX) between the system and the environment and the finite size device are considered in the FTT [1–11,56–59], therefore, the result obtained is closer to the actual HEG performance

Considering the heat transfer loss, Shen et al. [60] established an endoreversible SFLC model with constant-temperature HRs by applying FTT theory, analyzed the influences of HR temperature ratio and total heat conductance (HTC) on the power output (P) and efficiency (η) characteristics, and obtained the maximum P and maximum η and the corresponding optimal HTC distributions. Based on the NSGA-II algorithm, Ahmadi et al. [61] optimized the ecological performance coefficient and thermoeconomic performance of the endoreversible SFLC with constant-temperature HRs. Based on the Ref. [60], Wang et al. [62] further considered the internal irreversibility loss, established the irreversible SFLC model and optimized its P and η performance.

The above-mentioned were all studies on the SFLC with constant temperature HR. Based on Refs. [60–62], an irreversible SFLC with a variable temperature HR will be established in this paper, and the influence of internal irreversibility, HR inlet temperature ratio, thermal capacity rate (TCR) matching, and total HTC on cycle performance will be studied.

2. Cycle Model and Thermodynamic Performance

Figure 1 shows the T-s diagram of an irreversible variable temperature HR SFLC. Process $1 \to 2$ ($3 \to 1$) is a constant volume (pressure) endothermic (exothermic) one, and process $2 \to 3$ is an irreversible expansion one ($2 \to 3s$ is the corresponding isentropic one). Assuming the cycle working fluid is an ideal gas, as well as the inlet (outlet) temperature of the hot- and the cold-side fluid are $T_{Hin}(T_{Hout})$ and $T_{Lin}(T_{Lout})$.

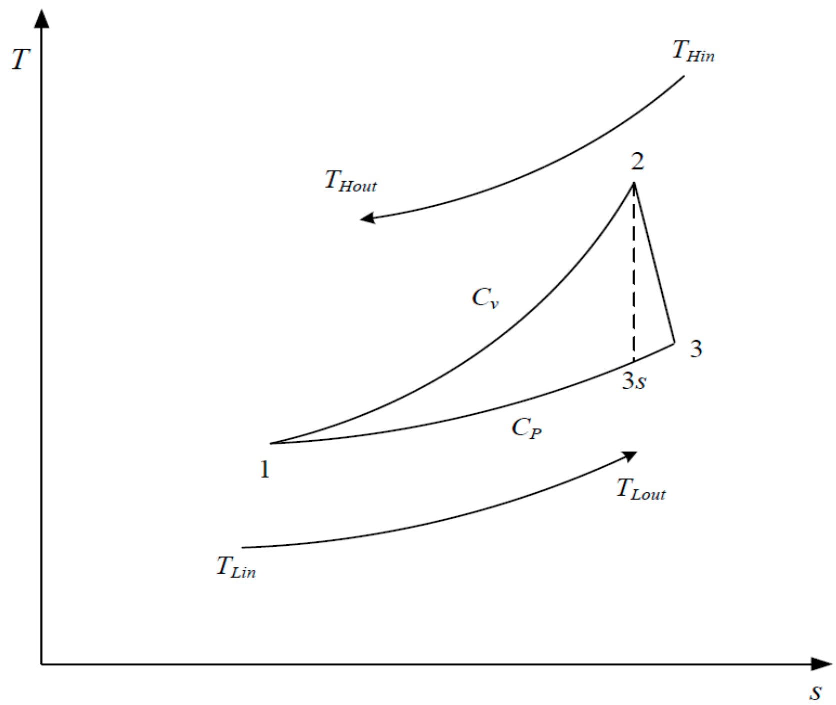

Figure 1. Cycle T-s diagram.

The irreversible expansion efficiency (η_e) is defined as [41,44,46,51]:

$$\eta_e = \frac{T_2 - T_3}{T_2 - T_{3s}} \tag{1}$$

Assuming the heat transfer between the working fluid and HR obeys the law of Newton heat transfer, according to the ideal gas properties and the theory of HEX, the cycle heat absorption and heat release rates are, respectively:

$$Q_H = C_{wf1}(T_2 - T_1) = C_{H\min}E_{H1}(T_{Hin} - T_1) \tag{2}$$

$$Q_L = C_{wf2}(T_3 - T_1) = C_{L\min}E_{L1}(T_3 - T_{Lin}) \tag{3}$$

where $C_H(C_L)$ and $C_{wf1}(C_{wf2})$ are heat source and working fluid TCRs ($C_{wf1} = \dot{m}C_v$, $C_{wf2} = \dot{m}C_P = kC_{wf1}$), respectively, $\dot{m}$ is the working fluid mass flow rate, $C_v(C_P)$ is the constant volume (pressure) specific heat, k is the specific heat ratio. E_{H1} and E_{L1} are the effectiveness of hot- and cold-side HEXs, respectively:

$$E_{H1} = \frac{1 - e^{-N_{H1}(1 - C_{H\min}/C_{H\max})}}{1 - (C_{H\min}/C_{H\max})e^{-N_{H1}(1 - C_{H\min}/C_{H\max})}} \tag{4}$$

$$E_{L1} = \frac{1 - e^{-N_{L1}(1 - C_{L\min}/C_{L\max})}}{1 - (C_{L\min}/C_{L\max})e^{-N_{L1}(1 - C_{L\min}/C_{L\max})}} \tag{5}$$

where N_{H1} and N_{L1} are the heat transfer unit number of the two HEXs, $C_{H\max}(C_{H\min})$ is the larger (smaller) of C_H and C_{wf1}, and $C_{L\max}(C_{L\min})$ is the larger (smaller) of C_L and kC_{wf1}. Their expressions are, respectively:

$$N_{H1} = \frac{U_H}{C_{H\min}} \tag{6}$$

$$N_{L1} = \frac{U_L}{C_{L\min}} \tag{7}$$

$$C_{H\max} = \max\left\{C_H, C_{wf1}\right\}, C_{H\min} = \min\left\{C_H, C_{wf1}\right\} \tag{8}$$

$$C_{L\max} = \max\left\{C_L, kC_{wf1}\right\}, C_{L\min} = \min\left\{C_L, kC_{wf1}\right\} \tag{9}$$

According to the second law of thermodynamics, one obtained:

$$\frac{T_2}{T_1} = \left(\frac{T_{3s}}{T_1}\right)^k \tag{10}$$

From Equations (2) and (3), the expressions of T_2 and T_3 are, respectively:

$$T_2 = \frac{C_{H\min}}{C_{wf1}}E_{H1}(T_{Hin} - T_1) + T_1 \tag{11}$$

$$T_3 = \frac{C_{L\min}E_{L1}T_{Lin} - kC_{wf1}T_1}{C_{L\min}E_{L1} - kC_{wf1}} \tag{12}$$

From Equations (1) and (10)–(12), the expression of T_1 can be obtained as:

$$T_1 = \frac{[(C_{L\min}E_L T_{Lin} - C_{wf2}T_1)/(C_{L\min}E_L - C_{wf2})] + [(C_{H\min}/C_{wf1})E_H(T_{Hin} - T_1) + T_1](\eta_e - 1)}{[(C_{H\min}/C_{wf1})E_H(T_{Hin} - T_1) + T_1]^{\frac{1}{k}} T_1^{-\frac{1}{k}}\eta_e} \tag{13}$$

From to Equations (2), (3), and (11)–(13), the expressions of P and η can be obtained as:

$$P = Q_H - Q_L = \frac{C_{H\min}E_{H1}(T_{Hin} - T_1)(C_{L\min}E_{L1} - kC_{wf1}) - kC_{L\min}E_{L1}C_{wf1}(T_{Lin} - T_1)}{C_{L\min}E_{L1} - kC_{wf1}} \tag{14}$$

$$\eta = P/\dot{Q}_H = \frac{C_{H\min}E_{H1}(T_{Hin} - T_1)(C_{L\min}E_{L1} - kC_{wf1}) - kC_{L\min}E_{L1}C_{wf1}(T_{Lin} - T_1)}{C_{H\min}E_{H1}(C_{L\min}E_{L1} - kC_{wf})(T_{Hin} - T_1)} \quad (15)$$

When $\eta_e = 1$, substituting into Equation (13), the expression of T_1 for an endoreversible SFLC with variable temperature HR can be obtained as:

$$T_1 = \frac{(C_{L\min}E_{L1}T_{Lin} - kC_{wf1}T_1)}{(C_{L\min}E_{L1} - kC_{wf1})\left\{[(C_{H\min}E_{H1}/C_{wf1})(T_{Hin} - T_1) + T_1]^{\frac{1}{k}}T_1^{-\frac{1}{k}}\right\}} \quad (16)$$

Combining Equations (4)–(9) and (14)–(16), by the numerical solution, the relationship between the P and η characteristics of the variable temperature HR endoreversible SFLC can be obtained.

Substituting $C_H = C_L \to \infty$ into Equations (4), (5) and (13)–(15) yields the expressions of the effectiveness of the two HEXs, P, η, and T_1 for an irreversible SFLC with constant temperature HR [62]:

$$E_H = 1 - \exp(-N_H) \quad (17)$$

$$E_L = 1 - \exp(-N_L) \quad (18)$$

$$T_1 = \frac{E_H T_H(\eta_e - 1) + (T_1 - E_L T_L)/(1 - E_L)}{\left\{(1 - E_H)(1 - \eta_e) + \{[E_H T_H + (1 - E_H)T_1]/T_1\}^{\frac{1}{k}}\eta_e\right\}} \quad (19)$$

$$P = \dot{Q}_{1\to2} - \dot{Q}_{3\to1} = \dot{m}C_v[E_H(T_H - T_1) - \frac{kE_L(T_1 - T_L)}{1 - E_L}] \quad (20)$$

$$\eta = P/\dot{Q}_{1\to2} = 1 - \frac{kE_L(T_1 - T_L)}{E_H(1 - E_L)(T_H - T_1)} \quad (21)$$

When $\eta_e = 1$ and $C_H = C_L \to \infty$, all of the expressions become the results of an endoreversible SFLC with constant temperature HR [60].

3. Numerical Examples and Discussions

3.1. Cycle Performance Analysis When the HTC of Hot- and Cold-Side HEXs Is Constant

Determining the relevant parameters according to the Refs. [53,60–62]: $C_v = 0.7165\ \mathrm{kJ/(kg \cdot K)}$, $\dot{m} = 1.1165\ \mathrm{kg/s}$, $T_L = 300K$, $C_H = C_L = 1.2$, $k = 1.4$, and $\eta_e = 0.92$.

Because the LC lacks an adiabatic compression process, it is a three-branch cycle, missing constraints on cycle pressure ratio, and the basic optimization relationship between P and η cannot be obtained. When U_H and U_L are given, it can be seen from Equations (4)–(7) and (13)–(15), when the corresponding effectiveness of HEXs and HR inlet temperature are given, the cycle P and η can be obtained as a certain point. Figure 2 shows the P-η characteristic of the cycle. It can be seen that when E_{H1} and E_{L1} take 0.8 and 0.9, as well as the HR inlet temperature ratio τ ($\tau = T_{Hin}/T_{Lin}$) are 3.25 and 3.75, respectively, the corresponding P-η show a "point" change. Parameters U_H, U_L, τ and η_e have significant effects on P and η. When U_H, U_L, τ, and η_e increase, P and η increase. When η_e changes from 0.75 to 1, P and η increase by about 639.3 and 632.2%, respectively.

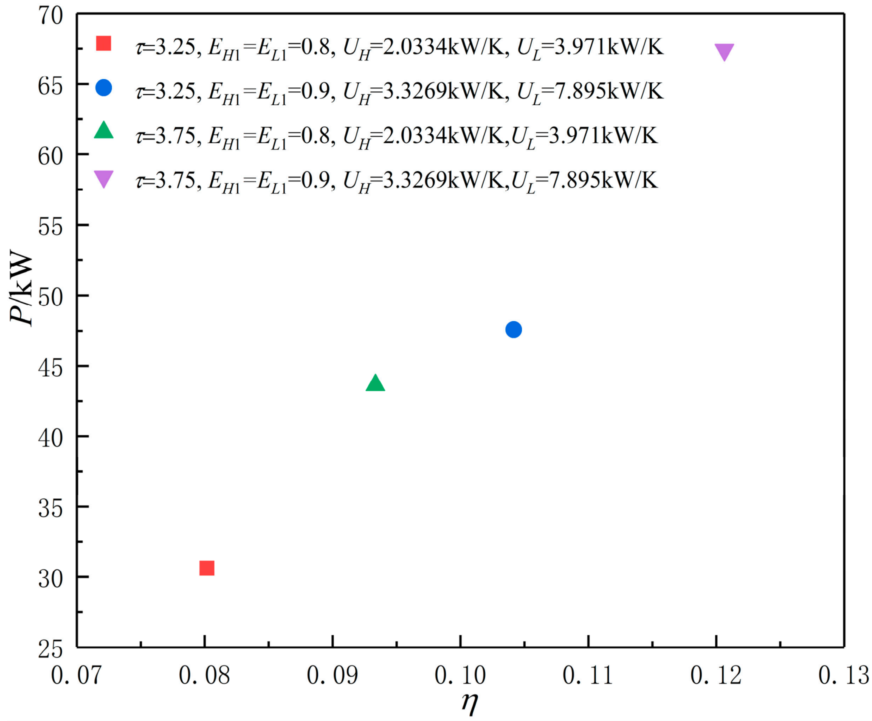

(**a**) The characteristics of P-η .

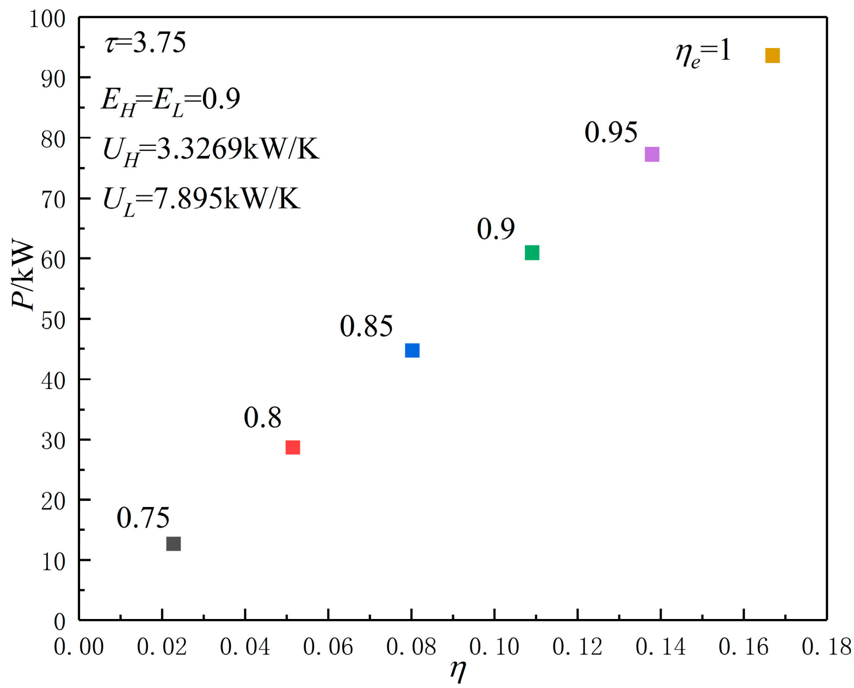

(**b**) The characteristics of P-η about η_e .

Figure 2. The characteristic of P-η (**a**) and the influence of η_e on P-η characteristics when U_H and U_L are given (**b**).

3.2. Cycle Performance Optimization When the HTC Distributions of the Two HEXs Can Be Optimized

Assuming that the sum of the HTCs of the two HEXs are a constant value:

$$U_L + U_H = U_T \tag{22}$$

$$U_H = (1 - u_L)U_T,\ U_L = u_L U_T \tag{23}$$

where $u_L = U_L/U_T$ and $0 < u_L < 1$. Combining Equations (4)–(7), (22) and (23), E_{H1} and E_{L1} expressions are, respectively:

$$E_{H1} = \frac{1 - e^{-[(1-u_L)U_T/C_{H\min}](1-C_{H\min}/C_{H\max})}}{1 - (C_{H\min}/C_{H\max})e^{-[(1-u_L)U_T/C_{H\min}](1-C_{H\min}/C_{H\max})}} \tag{24}$$

$$E_{L1} = \frac{1 - e^{-(u_L U_T/C_{L\min})(1-C_{L\min}/C_{L\max})}}{1 - (C_{L\min}/C_{L\max})e^{-(u_L U_T/C_{L\min})(1-C_{L\min}/C_{L\max})}} \tag{25}$$

Combining Equations (13)–(15) and (24)–(25), the relationships between P and η versus u_L of the irreversible SFLC with variable temperature HR can be obtained.

Figures 3 and 4 show the P and η versus u_L characteristics when u_L can be optimized. The two figures show that the characteristics of P-u_L and η-u_L are parabolic-like ones, that is, there are maximum P ($P_{\max}$) and maximum η ($\eta_{\max}$) as well as the corresponding optimal HTC distributions ($u_{L_{P(opt)}}$ and $u_{L_{\eta(opt)}}$).

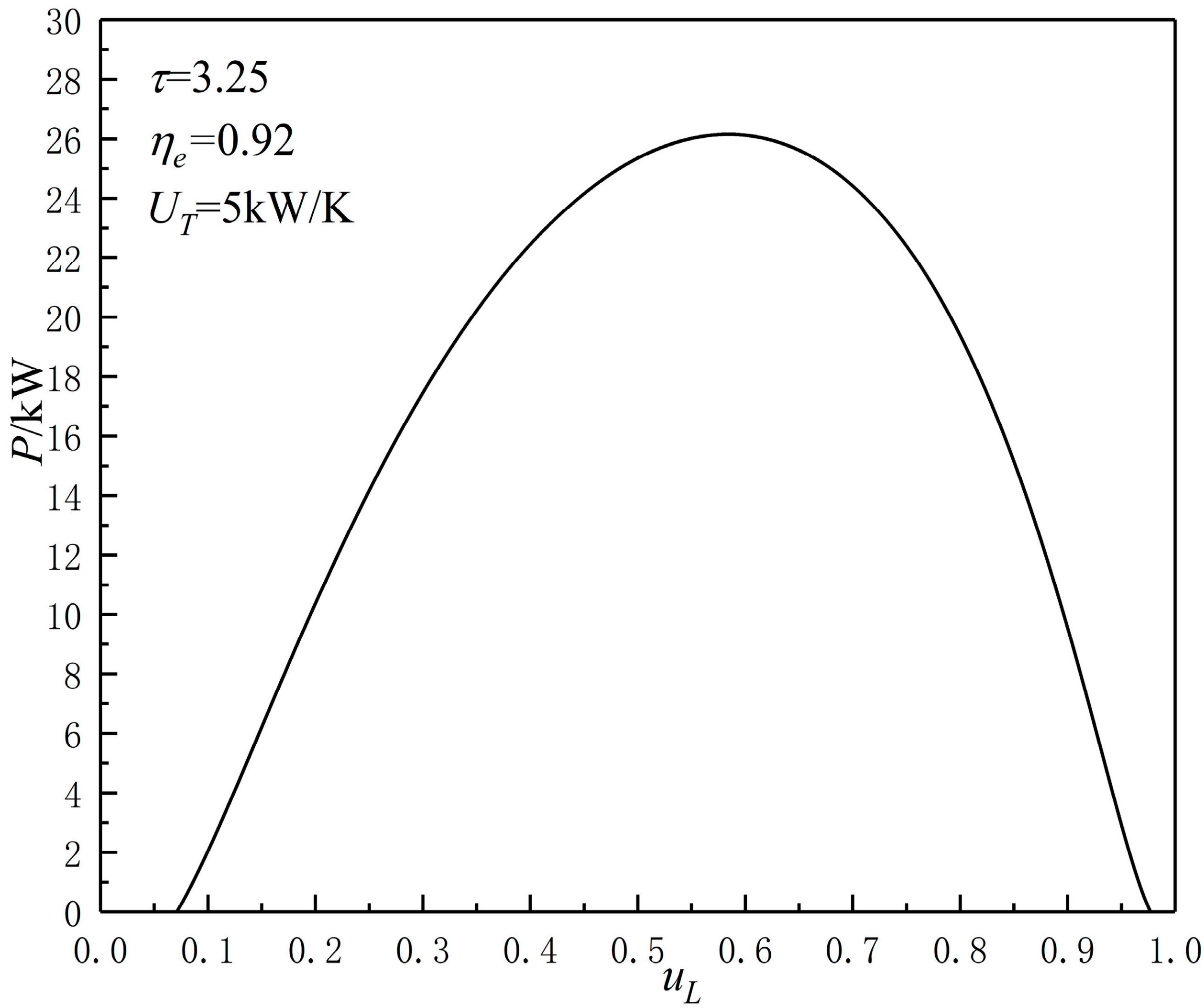

Figure 3. The curve of P-u_L.

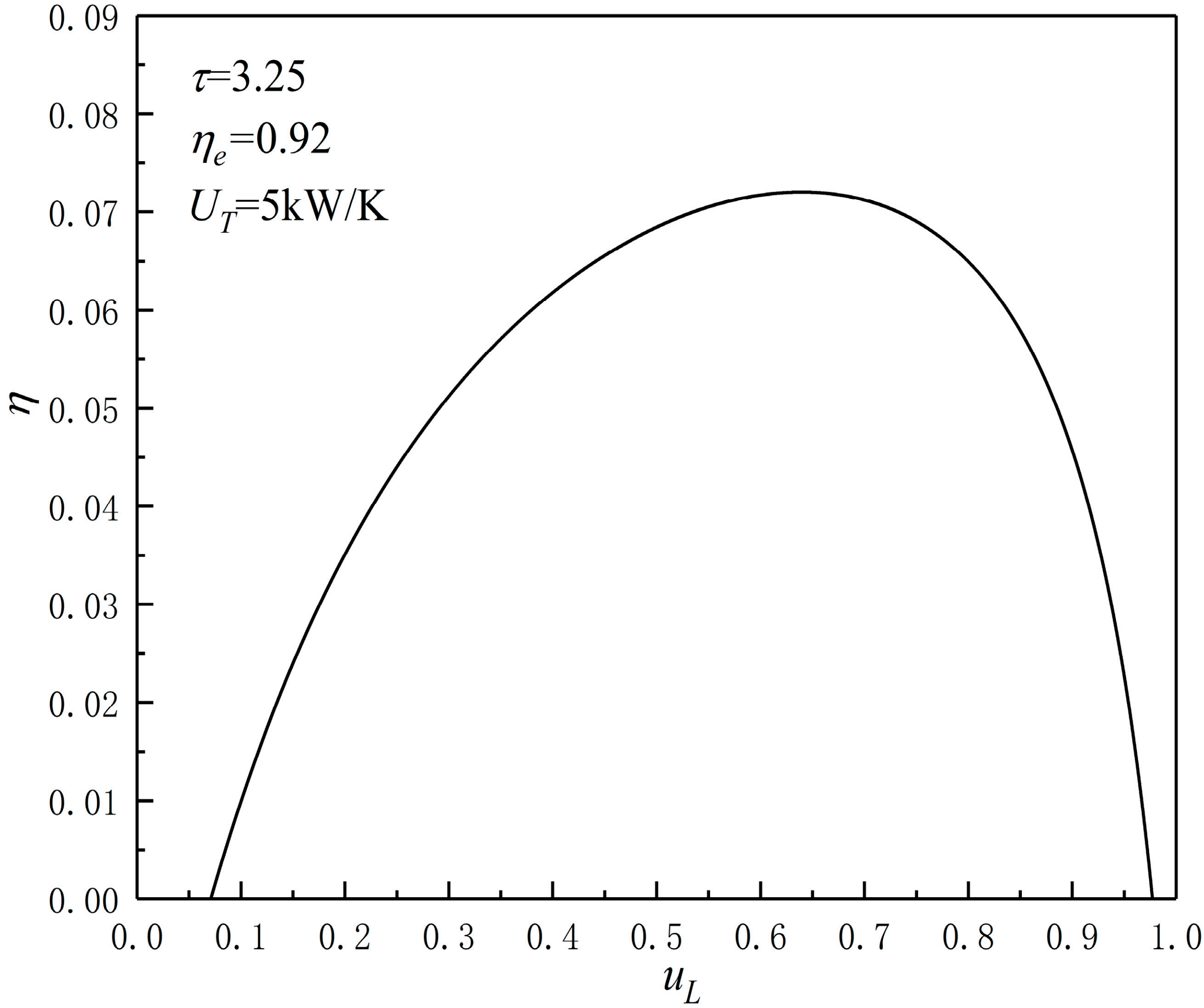

Figure 4. The curve of η-u_L.

Figures 5–8 show the influences of τ, U_T, and η_e on $P_{\max}$, $\eta_{\max}$, $u_{L_P(opt)}$, and $u_{L_\eta(opt)}$. It can be seen from Figures 5 and 6, when τ is fixed and as U_T increases, $P_{\max}$ and $\eta_{\max}$ increase, $u_{L_P(opt)}$ and $u_{L_\eta(opt)}$ first increase and then decrease; when U_T is fixed and as τ increases, $P_{\max}$, $\eta_{\max}$, $u_{L_P(opt)}$, and $u_{L_\eta(opt)}$ increase; according to Figures 7 and 8, with the increases of η_e, $P_{\max}$, and $\eta_{\max}$ increase, $u_{L_P(opt)}$ and $u_{L_\eta(opt)}$ decrease.

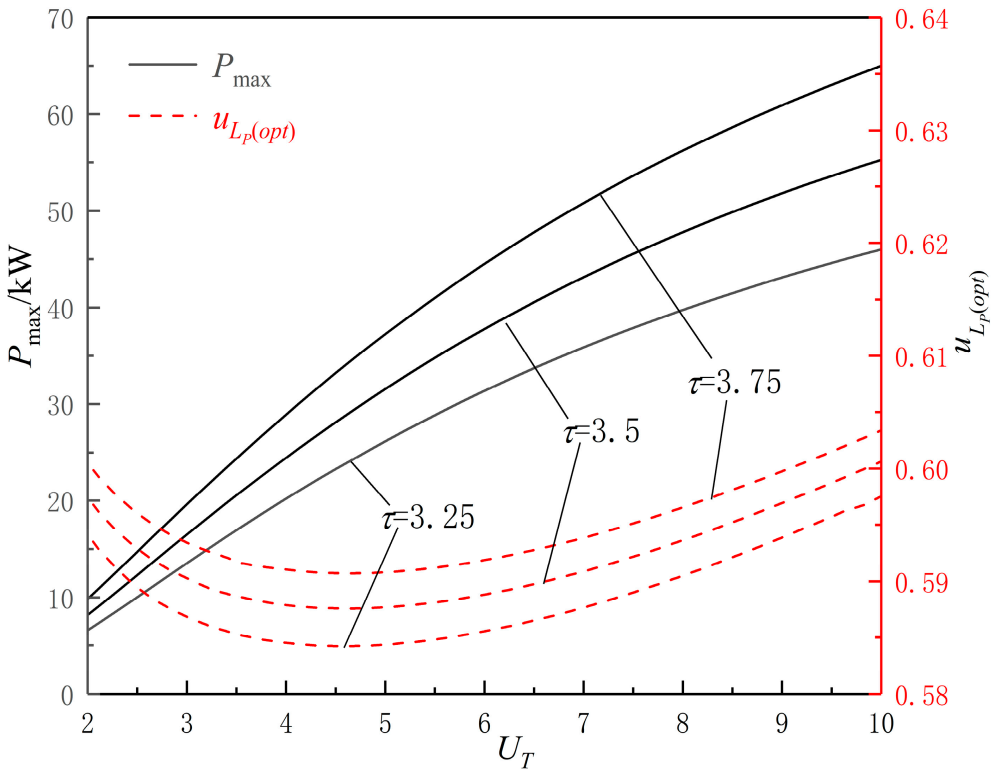

Figure 5. The characteristics of $P_{\max}$-U_T and $u_{L_{P}(opt)}$-U_T about τ.

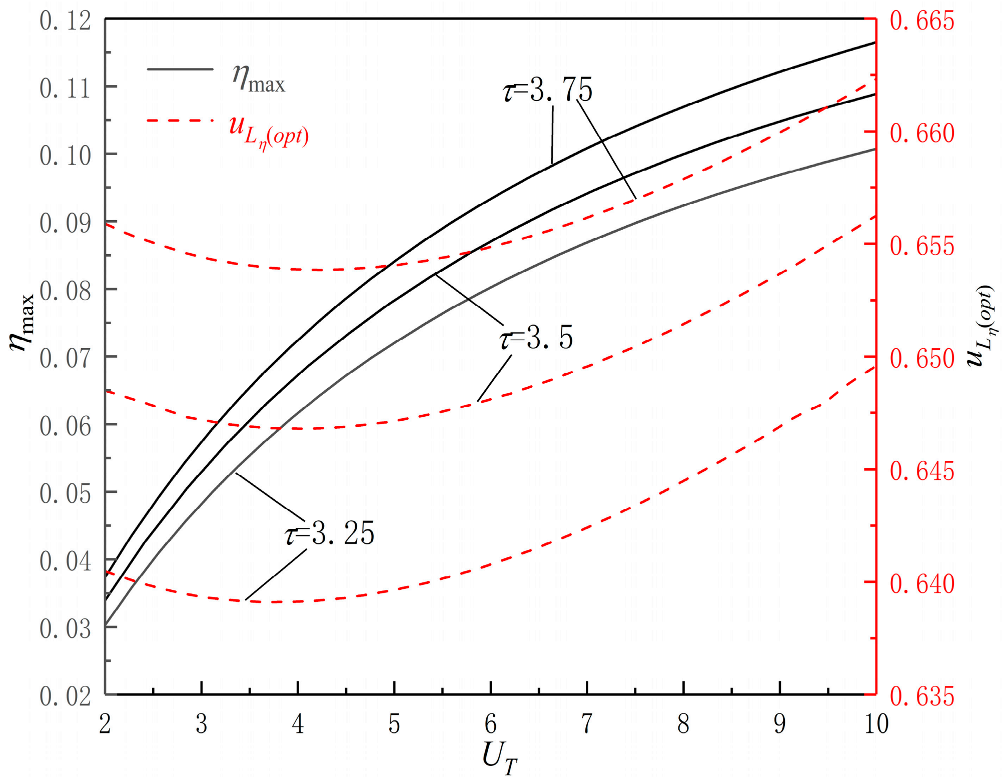

Figure 6. The characteristics of $\eta_{\max}$-U_T and $u_{L_{\eta}(opt)}$-U_T about τ.

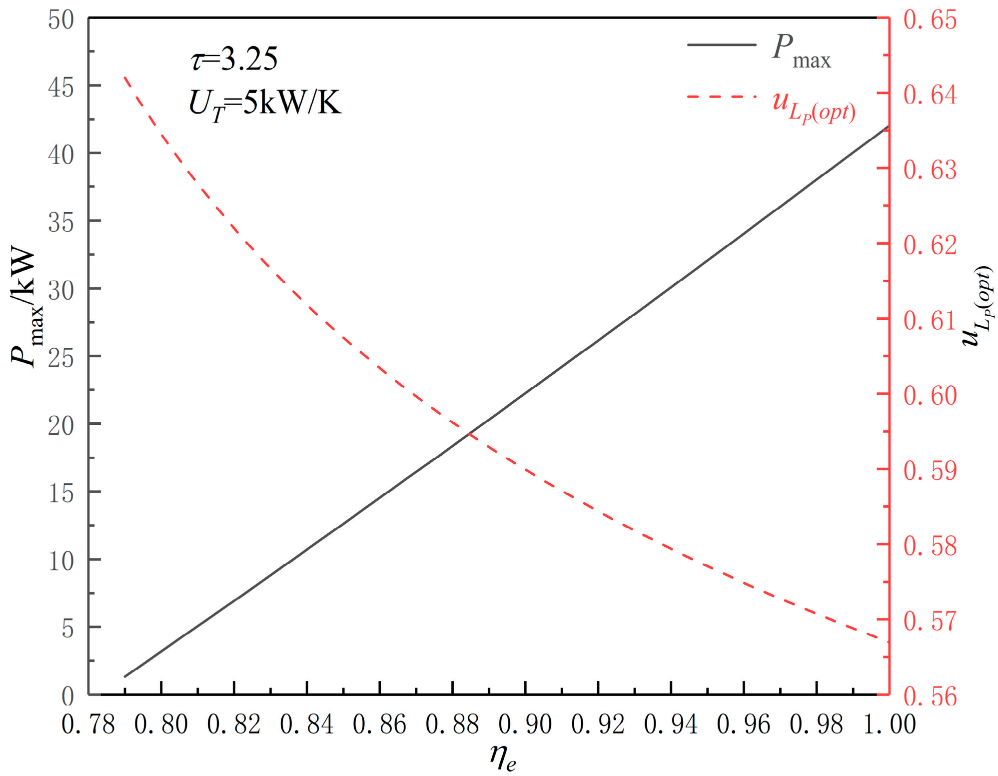

Figure 7. The characteristics of P_{max}-η_e and $u_{L_P(opt)}$-η_e.

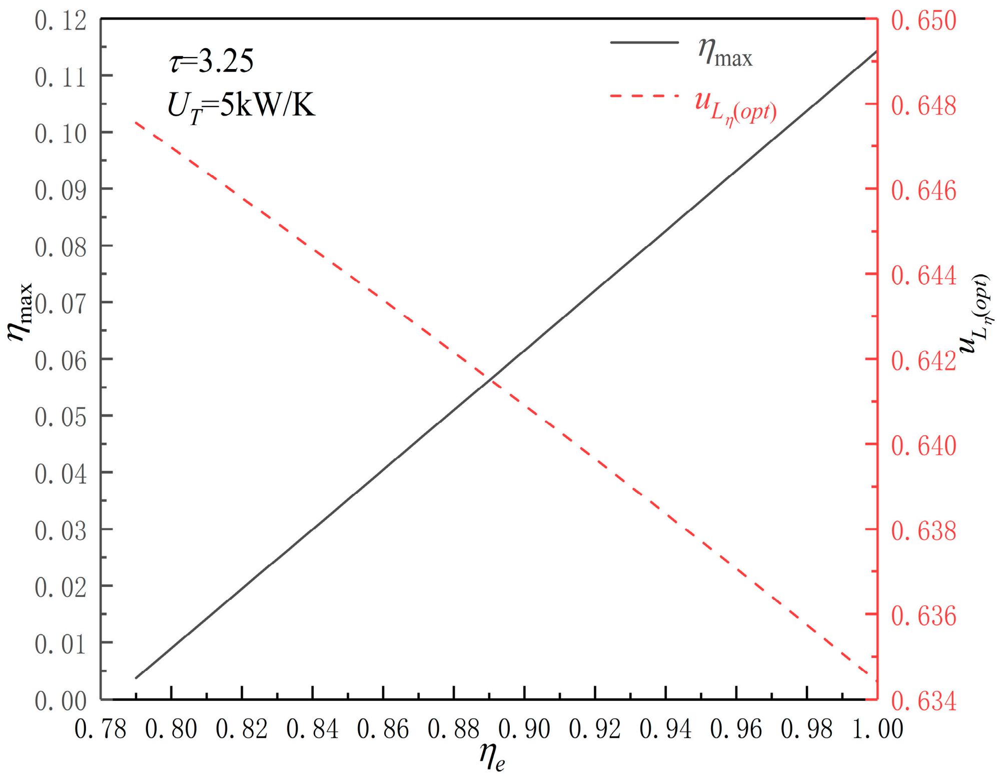

Figure 8. The characteristics of η_{max}-η_e and $u_{L_\eta(opt)}$-η_e.

3.3. TCR Matching Optimization

Setting $C_H = 1.2$, $\tau = 3.25$, $U_T = 5$ kW/K, and $C_L/C_H = 1$, and taking P as the objective function and u_L as the optimization variable, the influences of HR TCR ratio (C_L/C_H), U_T and τ on the characteristics of $P_{\max}$-C_{wf1}/C_H were studied.

Figures 9–12 show the influences of the C_L/C_H, U_T, τ and η_e on the characteristics of $P_{\max}$-C_{wf1}/C_H. It can be seen that with the increases of C_{wf1}/C_H, $P_{\max}$-C_{wf1}/C_H shows a parabolic-like change that first increases and then decreases, that is, there is an optimal $C_{wf1}/C_H((C_{wf1}/C_H)_{opt})$ which makes the cycle reach double-maximum power point $((P_{\max})_{\max})$.

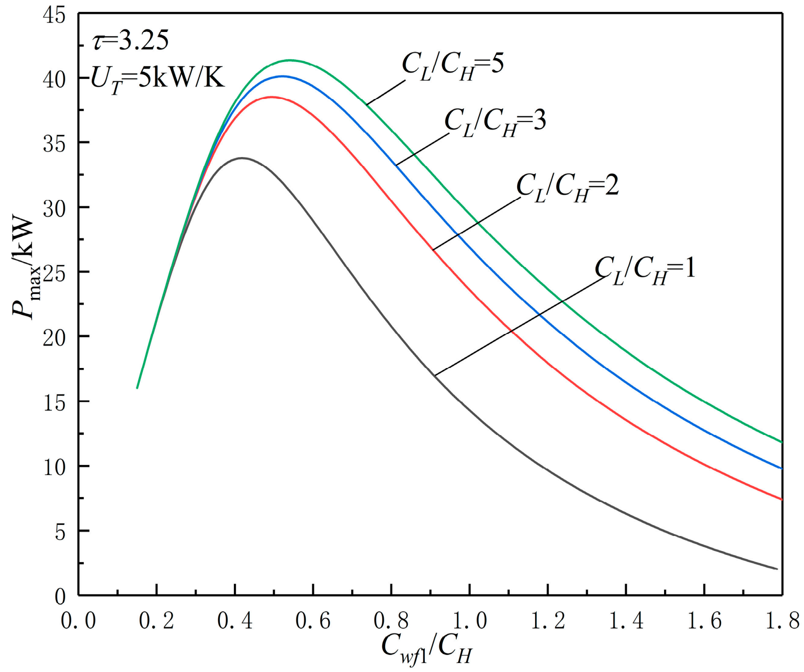

Figure 9. The characteristics of $P_{\max}$-C_{wf1}/C_H about C_L/C_H.

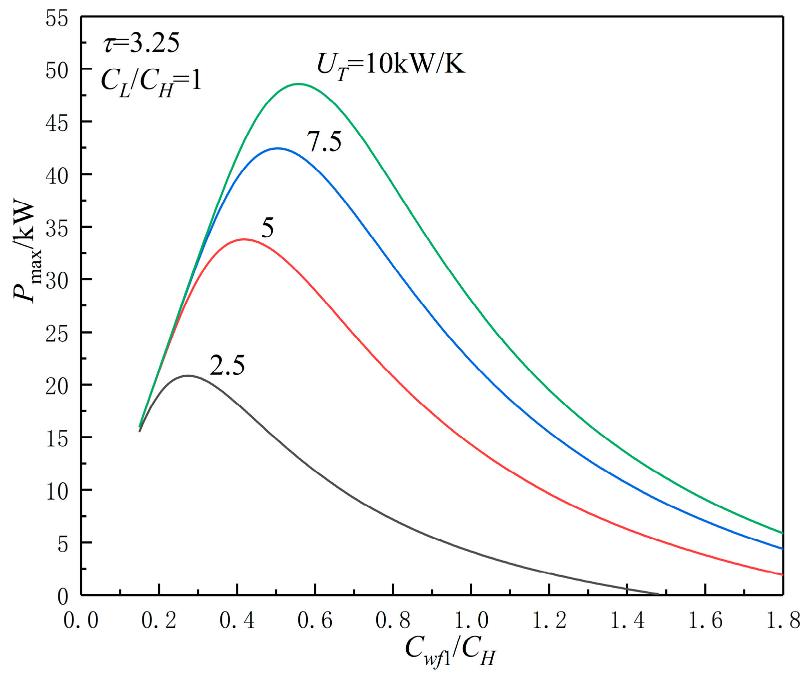

Figure 10. The characteristics of $P_{\max}$-C_{wf1}/C_H about U_T.

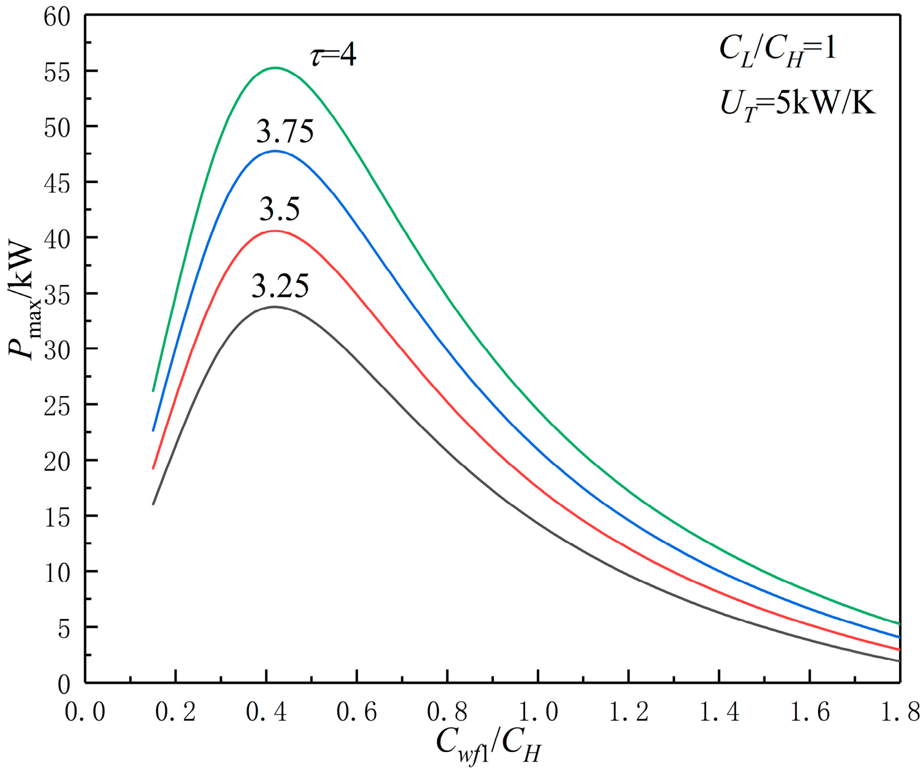

Figure 11. The characteristics of $P_{\max}$-C_{wf1}/C_H about τ.

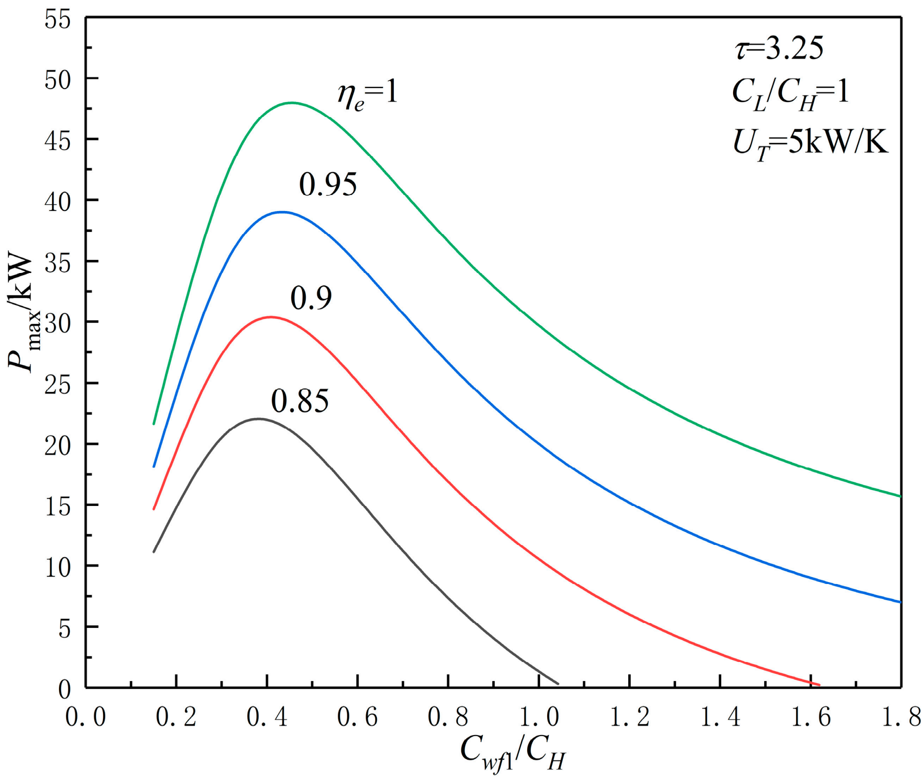

Figure 12. The characteristics of $P_{\max}$-C_{wf1}/C_H about η_e.

Figure 9 shows the influence of C_L/C_H on the characteristics of $P_{\max}$-C_{wf1}/C_H. As can be seen, with the increase of C_L/C_H, $(P_{\max})_{\max}$ and $(C_{wf1}/C_H)_{opt}$ increase. When C_L/C_H takes 1, 2, 3, and 5, $(P_{\max})_{\max}$ is 33.78, 38.52, 40.11, and 41.37 kW, and $(C_{wf1}/C_H)_{opt}$ is 0.42, 0.49, 0.52, and 0.54, respectively. C_L/C_H increases from 1 to 5, $(P_{\max})_{\max}$ increases by about 22.5%, $(C_{wf1}/C_H)_{opt}$ increases by about 28.6%.

Figure 10 shows the influence of U_T on the characteristics of $P_{\max}$-C_{wf1}/C_H. When U_T increases, $(P_{\max})_{\max}$ and $(C_{wf1}/C_H)_{opt}$ increase. When U_T takes 2.5, 5, 7.5, and 10 kW/K, $(P_{\max})_{\max}$ are 20.84, 33.78, 42.44, and 48.56 kW, and $(C_{wf1}/C_H)_{opt}$ is 0.27, 0.42, 0.50, and 0.56, respectively. When U_T increases from 2.5 to 10 kW/K, $(P_{\max})_{\max}$ and $(C_{wf1}/C_H)_{opt}$ increase by about 133.01% and 107.4%, respectively.

Figure 11 shows the influence of τ on the characteristics of $P_{\max}$-C_{wf1}/C_H. When τ increases, $(P_{\max})_{\max}$ increases and $(C_{wf1}/C_H)_{opt}$ is unchanged. When τ takes 3.25, 3.5, 3.75, and 4, $(P_{\max})_{\max}$ is 33.78, 40.58, 47.75, and 55.25 kW, respectively, and $(C_{wf1}/C_H)_{opt}$ is 0.42. When τ increases from 3.25 to 4, $(P_{\max})_{\max}$ increases by about 63.6%.

Figure 12 shows the influence of η_e on the characteristics of $P_{\max}$-C_{wf1}/C_H. When η_e increases, $(P_{\max})_{\max}$ and $(C_{wf1}/C_H)_{opt}$ increase. When η_e takes 0.85, 0.9, 0.95, and 1, $(P_{\max})_{\max}$ is 22.06, 30.36, 39.01, and 47.97 kW, $(C_{wf1}/C_H)_{opt}$ is 0.38, 0.41, 0.43, and 0.46, respectively. When η_e increases from 0.85 to 1, $(P_{\max})_{\max}$ increases by about 117.5%, and $(C_{wf1}/C_H)_{opt}$ increases by about 21.1%.

4. Conclusions

In this paper, an irreversible SFLC model with variable temperature HR is established by applying FTT theory, the expressions of P and η are derived, and the influences of U_T, τ, C_L/C_H, η_e, and C_{wf1}/C_H on P and η performances are analyzed. The results show that:

(1) When U_H and U_L are constants, P-η is a certain "point", and with the increases in τ, U_H, U_L, and η_e, P and η increase. When u_L can be optimized, P and η versus u_L characteristics are parabolic-like ones, there are $u_{L_P(opt)}$ and $u_{L_\eta(opt)}$ which makes the cycle reach $P_{\max}$ and $\eta_{\max}$.

(2) With the increase of C_{wf1}/C_H, $P_{\max}$-C_{wf1}/C_H show a parabolic-like change, there is an $(C_{wf1}/C_H)_{opt}$, which makes the cycle reach $(P_{\max})_{\max}$. With the increases in C_L/C_H, U_T, and η_e, $(P_{\max})_{\max}$ and $(C_{wf1}/C_H)_{opt}$ increase. With the increases in τ, $(P_{\max})_{\max}$ increases, and $(C_{wf1}/C_H)_{opt}$ is unchanged.

(3) Internal irreversibility and variable temperature HR are two general properties of practical cycles. It is necessary to study their influences on the cycle performance. FTT is a powerful theoretical tool for thermodynamic cycles with those properties.

Author Contributions: Conceptualization, R.W. and L.C.; data curation, Y.G.; funding acquisition, L.C.; methodology, R.W., Y.G., L.C., and H.F.; software, R.W., Y.G., and H.F.; supervision, L.C.; validation, R.W. and H.F.; writing—original draft preparation, R.W. and Y.G.; writing—reviewing and Editing, L.C. All authors have read and agreed to the published version of the manuscript.

Funding: This paper is supported by The National Natural Science Foundation of China (Project No. 51779262) and The Graduate Innovative Fund of Wuhan Institute of Technology (Project Nos. CX2020044 and CX2020047).

Institutional Review Board Statement: Not applicable.

Informed Consent Statement: Not applicable.

Acknowledgments: The authors wish to thank the reviewers for their careful, unbiased and constructive suggestions, which led to this revised manuscript.

Conflicts of Interest: The authors declare no conflict of interest.

Nomenclature

C_P	specific heat at constant pressure $(\text{kJ}/(\text{kg} \cdot \text{K}))$
C_v	specific heat at constant volume $(\text{kJ}/(\text{kg} \cdot \text{K}))$
E	effectiveness of heat exchanger
k	specific heat ratio (-)
$\dot{m}$	mass flow rate of the working fluid (kg/s)
N	number of heat transfer units
P	cycle power (kW)
$\dot{Q}$	quantity of heat transfer rate (kW)
T	temperature (K)
U	heat conductance (kW/K)
U_T	total heat conductance (kW/K)
u	heat conductance distribution
Greek symbols	
τ	heat reservoirs inlet temperature ratio
η	cycle thermal efficiency
Subscripts	
H	hot-side
L	cold-side
max	maximum value
opt	optimal
P	maximum power point
η	maximum thermal efficiency point
1-3, 3s	cycle state points

Abbreviations

FTT	finite-time thermodynamic
HEG	heat engine
HEX	heat exchanger
HR	heat reservoirs
HTC	heat conductance
LC	Lenoir cycle
SFLC	steady flow Lenoir cycle
TCR	thermal capacity rate

References

1. Andresen, B. *Finite-Time Thermodynamics*; Physics Laboratory II, University of Copenhagen: Copenhagen, Danmark, 1983.
2. Hoffmann, K.H.; Burzler, J.M.; Schubert, S. Endoreversible thermodynamics. *J. Non-Equilib. Thermodyn.* **1997**, *22*, 311–355.
3. Chen, L.G.; Wu, C.; Sun, F.R. Finite time thermodynamic optimization or entropy generation minimization of energy systems. *J. Non-Equilib. Thermodyn.* **1999**, *24*, 327–359. [CrossRef]
4. Andresen, B. Current trends in finite-time thermodynamics. *Angew. Chem. Int. Ed.* **2011**, *50*, 2690–2704. [CrossRef]
5. Ge, Y.L.; Chen, L.G.; Sun, F.R. Progress in finite time thermodynamic studies for internal combustion engine cycles. *Entropy* **2016**, *18*, 139. [CrossRef]
6. Feidt, M. The history and perspectives of efficiency at maximum power of the Carnot engine. *Entropy* **2017**, *19*, 369. [CrossRef]
7. Feidt, M.; Costea, M. Progress in Carnot and Chambadal modeling of thermomechanical engine by considering entropy and heat transfer entropy. *Entropy* **2019**, *21*, 1232. [CrossRef]
8. Diskin, D.; Tartakovsky, L. Efficiency at maximum power of the low-dissipation hybrid electrochemical-Otto cycle. *Energies* **2020**, *13*, 3961. [CrossRef]
9. Lucia, U.; Grisolia, G.; Kuzemsky, A.L. Time, irreversibility and entropy production in nonequilibrium systems. *Entropy* **2020**, *22*, 887. [CrossRef] [PubMed]
10. Costea, M.; Petrescu, S.; Feidt, M.; Dobre, C.; Borcila, B. Optimization modeling of irreversible Carnot engine from the perspective of combining finite speed and finite time analysis. *Entropy* **2021**, *23*, 504. [CrossRef]
11. Berry, R.S.; Salamon, P.; Andresen, B. How it all began. *Entropy* **2020**, *22*, 908. [CrossRef]
12. Meng, Z.W.; Chen, L.G. Theoretical maximum efficiency and higher power output in triboelectric nanogenerators. *Energy Rep.* **2020**, *6*, 2463–2475. [CrossRef]

13. Chen, L.G.; Meng, Z.W.; Ge, Y.L.; Wu, F. Performance analysis and optimization for irreversible combined quantum Carnot heat engine working with ideal quantum gases. *Entropy* **2021**, *23*, 536. [CrossRef] [PubMed]
14. Qi, C.Z.; Ding, Z.M.; Chen, L.G.; Ge, Y.L.; Feng, H.J. Modeling and performance optimization of an irreversible two-stage combined thermal Brownian heat engine. *Entropy* **2021**, *23*, 419. [CrossRef] [PubMed]
15. Qi, C.Z.; Ding, Z.M.; Chen, L.G.; Ge, Y.L.; Feng, H.J. Modelling of irreversible two-stage combined thermal Brownian refrigerators and their optimal performance. *J. Non-Equilib. Thermodyn.* **2021**, *46*, 175–189. [CrossRef]
16. Pourkiaei, S.M.; Ahmadi, M.H.; Sadeghzadeh, M.; Moosavi, S.; Pourfayaz, F.; Chen, L.G.; Yazdi, M.A.; Kumar, R. Thermoelectric cooler and thermoelectric generator devices: A review of present and potential applications, modeling and materials. *Energy* **2019**, *186*, 115849. [CrossRef]
17. Chen, L.G.; Meng, F.K.; Ge, Y.L.; Feng, H.J.; Xia, S.J. Performance optimization of a class of combined thermoelectric heating devices. *Sci. China Technol. Sci.* **2020**, *63*, 2640–2648. [CrossRef]
18. Qiu, S.S.; Ding, Z.M.; Chen, L.G.; Ge, Y.L. Performance optimization of thermionic refrigerators based on van der Waals heterostructures. *Sci. China Technol. Sci.* **2021**, *64*, 1007–1016. [CrossRef]
19. Qiu, S.S.; Ding, Z.M.; Chen, L.G. Performance evaluation and parametric optimum design of irreversible thermionic generators based on van der Waals heterostructures. *Energy Convers. Manag.* **2020**, *225*, 113360. [CrossRef]
20. Tang, C.Q.; Feng, H.J.; Chen, L.G.; Wang, W.H. Power density analysis and multi-objective optimization for a modified endoreversible simple closed Brayton cycle with one isothermal heat process. *Energy Rep.* **2020**, *6*, 1648–1657. [CrossRef]
21. Chen, L.G.; Shen, J.F.; Ge, Y.L.; Wu, Z.X.; Wang, W.H.; Zhu, F.L.; Feng, H.J. Power and efficiency optimization of open Maisotsenko-Brayton cycle and performance comparison with traditional open regenerated Brayton cycle. *Energy Convers. Manag.* **2020**, *217*, 113001. [CrossRef]
22. Chen, L.G.; Tang, C.Q.; Feng, H.J.; Ge, Y.L. Power, efficiency, power density and ecological function optimizations for an irreversible modified closed variable-temperature reservoir regenerative Brayton cycle with one isothermal heating process. *Energies* **2020**, *13*, 5133. [CrossRef]
23. Chen, L.G.; Ge, Y.L.; Liu, C.; Feng, H.J.; Lorenzini, G. Performance of universal reciprocating heat-engine cycle with variable specific heats ratio of working fluid. *Entropy* **2020**, *22*, 397. [CrossRef]
24. Shi, S.S.; Ge, Y.L.; Chen, L.G.; Feng, H.J. Performance optimizations with single-, bi-, tri- and quadru-objective for irreversible Atkinson cycle with nonlinear variation of working fluid's specific heat. *Energies* **2021**, *14*, 4175. [CrossRef]
25. Feng, H.J.; Tao, G.S.; Tang, C.Q.; Ge, Y.L.; Chen, L.G.; Xia, S.J. Exergoeconomic performance optimization for a regenerative gas turbine closed-cycle heat and power cogeneration plant. *Energy Rep.* **2019**, *5*, 1525–1531. [CrossRef]
26. Chen, L.G.; Yang, B.; Feng, H.J.; Ge, Y.L.; Xia, S.J. Performance optimization of an open simple-cycle gas turbine combined cooling, heating and power plant driven by basic oxygen furnace gas in China's steelmaking plants. *Energy* **2020**, *203*, 117791. [CrossRef]
27. Li, J.; Chen, L.G. Exergoeconomic performance optimization of space thermoradiative cell. *Eur. Phys. J. Plus* **2021**, *136*, 644. [CrossRef]
28. Zhang, L.; Chen, L.G.; Xia, S.J.; Ge, Y.L.; Wang, C.; Feng, H.J. Multi-objective optimization for helium-heated reverse water gas shift reactor by using NSGA-II. *Int. J. Heat Mass Transf.* **2020**, *148*, 119025. [CrossRef]
29. Kong, R.; Chen, L.G.; Xia, S.J.; Li, P.L.; Ge, Y.L. Performance analysis of hydrogen iodide decomposition membrane reactor under different sweep modes. *Energy Convers. Manag.* **2021**, *244*, 114436. [CrossRef]
30. Chen, Y.R. Maximum profit configurations of commercial engines. *Entropy* **2011**, *13*, 1137–1151. [CrossRef]
31. Tsirlin, A.; Gagarina, L. Finite-time thermodynamics in economics. *Entropy* **2020**, *22*, 891. [CrossRef]
32. Agnew, B.; Walker, S.; Ng, B.; Tam, I.C.K. Finite time analysis of a tri-generation cycle. *Energies* **2015**, *8*, 6215–6229. [CrossRef]
33. Dumitrascu, G.; Feidt, M.; Popescu, A.; Grigorean, S. Endoreversible trigeneration cycle design based on finite physical dimensions thermodynamics. *Energies* **2019**, *12*, 3165.
34. Yasunaga, T.; Fontaine, K.; Ikegami, Y. Performance evaluation concept for ocean thermal energy conversion toward standardization and intelligent design. *Energies* **2021**, *14*, 2336. [CrossRef]
35. Dumitrașcu, G.; Feidt, M.; Grigorean, S. Finite physical dimensions thermodynamics analysis and design of closed irreversible cycles. *Energies* **2021**, *14*, 3416. [CrossRef]
36. Gonzalez-Ayala, J.; Roco, J.M.M.; Medina, A.; Calvo, H.A. Optimization, stability, and entropy in endoreversible heat engines. *Entropy* **2020**, *22*, 1323. [CrossRef] [PubMed]
37. Levario-Medina, S.; Valencia-Ortega, G.; Barranco-Jimenez, M.A. Energetic optimization considering a generalization of the ecological criterion in traditional simple-cycle and combined cycle power plants. *J. Non-Equilib. Thermodyn.* **2020**, *45*, 269–290. [CrossRef]
38. Rai, R.K.; Sahoo, R.R. Effective power and effective power density analysis for water in diesel emulsion as fuel in diesel engine performance. *Energy* **2019**, *180*, 893–902. [CrossRef]
39. Abedinnezhad, S.; Ahmadi, M.H.; Pourkiaei, S.M.; Pourfayaz, F.; Mosavi, A.; Feidt, M.; Shamshirband, S. Thermodynamic assessment and multi-objective optimization of performance of irreversible Dual-Miller cycle. *Energies* **2019**, *12*, 4000. [CrossRef]
40. Masser, R.; Hoffmann, K.H. Endoreversible modeling of a hydraulic recuperation system. *Entropy* **2020**, *22*, 383. [CrossRef]
41. Schwalbe, K.; Fischer, A.; Wagner, K.; Schmidt, K.; Hoffmann, K.H. Recuperation gain for a hydraulic energy storage in automotive applications. *Appl. Thermal Eng.* **2020**, *175*, 115275. [CrossRef]
42. Scheunert, M.; Masser, R.; Khodja, A.; Paul, R.; Schwalbe, K.; Fischer, A.; Hoffmann, K.H. Power-optimized sinusoidal piston motion and its performance gain for an Alpha-type Stirling engine with limited regeneration. *Energies* **2020**, *13*, 4564. [CrossRef]

43. Gonca, G.; Sahin, B.; Cakir, M. Performance assessment of a modified power generating cycle based on effective ecological power density and performance coefficient. *Int. J. Exergy* **2020**, *33*, 153–164. [CrossRef]
44. Shi, S.S.; Chen, L.G.; Ge, Y.L.; Feng, H.J. Performance optimizations with single-, bi-, tri- and quadru-objective for irreversible Diesel cycle. *Entropy* **2021**, *23*, 826. [CrossRef] [PubMed]
45. Ge, Y.L.; Chen, L.G.; Feng, H.J. Ecological optimization of an irreversible Diesel cycle. *Eur. Phys. J. Plus* **2021**, *136*, 198. [CrossRef]
46. Lai, H.Y.; Li, Y.T.; Chan, Y.H. Efficiency enhancement on hybrid power system composed of irreversible solid oxide fuel cell and Stirling engine by finite time thermodynamics. *Energies* **2021**, *14*, 1037. [CrossRef]
47. Masser, R.; Hoffmann, K.H. Optimal control for a hydraulic recuperation system using endoreversible thermodynamics. *Appl. Sci.* **2021**, *11*, 5001. [CrossRef]
48. Paul, R.; Hoffmann, K.H. Cyclic control optimization algorithm for Stirling engines. *Symmetry* **2021**, *13*, 873. [CrossRef]
49. Maheshwari, G.; Mehta, A.; Chaudhary, S.; Somani, S.K. Performance comparison of an irreversible closed variable temperature heat reservoir Carnot engine under maximum power density and maximum power conditions. *Int. J. Ambient Energy* **2006**, *27*, 65–77. [CrossRef]
50. Ust, Y.; Sogut, O.S.; Sahin, B.; Durmayaz, A. Ecological coefficient of performance (ECOP) optimization for an irreversible Brayton heat engine with variable-temperature thermal reservoirs. *J. Energy Inst.* **2006**, *79*, 47–52. [CrossRef]
51. Feidt, M.; Costea, M.; Feidt, R.; Danel, Q.; Périlhon, C. New criteria to characterize the waste heat recovery. *Energies* **2020**, *13*, 789. [CrossRef]
52. Yasunaga, T.; Noguchi, T.; Morisaki, T.; Ikegami, Y. Basic heat exchanger performance evaluation method on OTEC. *J. Mar. Sci. Eng.* **2018**, *6*, 32. [CrossRef]
53. Tang, C.Q.; Chen, L.G.; Feng, H.J.; Wang, W.H.; Ge, Y.L. Power optimization of a closed binary Brayton cycle with isothermal heating processesand coupled to variable-temperature reservoirs. *Energies* **2020**, *13*, 3212. [CrossRef]
54. Lichty, C. *Combustion Engine Processes*; McGraw-Hill: New York, NY, USA, 1967.
55. Georgiou, D.P. Useful work and the thermal efficiency in the ideal Lenoir with regenerative preheating. *J. Appl. Phys.* **2008**, *88*, 5981–5986. [CrossRef]
56. Andresen, B.; Salamon, P.; Berry, R.S. Thermodynamics in finite time. *Phys. Today* **1987**, *37*, 62–70. [CrossRef]
57. Berry, R.S.; Kazakov, V.A.; Sieniutycz, S.; Szwast, Z.; Tsirlin, A.M. *Thermodynamic Optimization of Finite Time Processes*; Wiley: Chichester, UK, 1999.
58. Feidt, M. Thermodynamics applied to reverse cycle machines, a review. *Int. J. Refrig.* **2010**, *33*, 1327–1342. [CrossRef]
59. Roach, T.N.F.; Salamon, P.; Nulton, J.; Andresen, B.; Felts, B.; Haas, A.; Calhoun, S.; Robinett, N.; Rohwer, F. Application of finite-time and control thermodynamics to biological processes at multiple scales. *J. Non-Equilib. Thermodyn.* **2018**, *43*, 193–210. [CrossRef]
60. Shen, X.; Chen, L.G.; Ge, Y.L.; Sun, F.R. Finite-time thermodynamic analysis for endoreversible Lenoir cycle coupled to constant-temperature heat reservoirs. *Int. J. Energy Environ.* **2017**, *8*, 272–278.
61. Ahmadi, M.H.; Nazari, M.A.; Feidt, M. Thermodynamic analysis and multi-objective optimisation of endoreversible Lenoir heat engine cycle based on the thermo-economic performance criterion. *Int. J. Ambient Energy* **2019**, *40*, 600–609. [CrossRef]
62. Wang, R.B.; Ge, Y.L.; Chen, L.G.; Feng, H.J.; Wu, Z.X. Power and thermal efficiency optimization of an irreversible steady-flow Lenoir cycle. *Entropy* **2021**, *23*, 425. [CrossRef] [PubMed]